Front. Mater. Sci. 2025, 19(2): 250722
https://doi.org/10.1007/s11706-025-0722-3

LETTER

Direct fabrication of few-layer graphene via molten salt-assisted magnesiothermic reduction

Jie Liu[1,2], Binfeng Pan[1,2], Zhimin Zhang (✉)[1], and Xuchen Lu[1]

ABSTRACT: Graphene materials like turbostratic graphene exhibit remarkable promise for an array of applications, spanning from electronic devices to aerospace technologies. It is essential to develop a fabrication method that is not only economical and efficient, but also environmentally sustainable. In this study, the molten salt-assisted magnesiothermic reduction (MSAMR) method is proposed for the synthesis of few-layer turbostratic graphene. K_2CO_3 serves as both the carbon source and the catalyst for graphitization, facilitating the formation of the graphene structure, while *in-situ* generated MgO nanoparticles exert confinement and templating effects on the growth of graphene. The molten salts used effectively prevent the aggregation and the Bernal stacking of graphene sheets, ensuring the few-layer and turbostratic structure. The synergistic effects of K_2CO_3, *in-situ* generated MgO, and molten salts guarantee the formation of few-layer turbostratic graphene at a relatively low temperature, characterized with 4–8 stacking layers, a mesopore-dominated microstructure, and a high degree of graphitization.

KEYWORDS: few-layer turbostratic graphene; magnesiothermic reduction; molten salt; potassium carbonate; graphitization; mesopore-dominated microstructure

Few-layer graphene has attracted tremendous attention because of its exceptional physical and chemical characteristics, including impressive surface area, excellent flexibility, and superior thermal conductivity [1–3]. To date, several approaches have been devised, including mechanical and liquid exfoliation [4], chemical vapor deposition (CVD) [5], chemical reduction of graphene oxide [6], epitaxial growth [7], organic synthesis, and other methods [8]. However, they have not been as scalable as the expectation of the industries due to the expensive equipment (e.g., the CVD method), the complex process (e.g., the oxidation–reduction method), and the involvement of highly corrosive/toxic reagents [9]. Therefore, it is still a challenge to explore a cost-effective, straightforward, and environment-friendly method for the fabrication of graphene materials.

Recently, the magnesiothermic reduction of carbon-containing compounds (e.g., carbon dioxide, carbonates, and graphene oxide) emerges as an encouraging process towards the rapid and scalable synthesis of graphene materials. Till now, graphene materials have been successfully synthesized via violent shock-wave-assisted or gentle homogeneous heat-assisted magnesiothermic reduction from various carbonates (e.g., CO_2 [10], $CaCO_3$ [11], and $3MgCO_3{\cdot}Mg(OH)_2{\cdot}3H_2O$ [12]) or biomass (e.g., egg shells [13] and oxalic acid [14]). However, the dissociation of the C−O bond is an exothermic process with the enthalpy only slightly lower than that of the famous Goldschmidt reaction (e.g., $2Al + Fe_2O_3 = Al_2O_3 + 2Fe$, $\Delta_r H = -850\ kJ{\cdot}mol^{-1}$ [14]), which is fierce and not easy to control. Another promising trend for the preparation of graphene materials is the application of the molten salt method (or the ionothermal method). Fechler et al. developed a facile "salt templating" method for the synthesis of few-layer graphene or porous carbon using low-melting-point eutectic molten salt (e.g., LiCl–$ZnCl_2$, NaCl–$ZnCl_2$, and KCl–$ZnCl_2$) as the solvent and porogen

1 State Key Laboratory of Mesoscience and Engineering, Institute of Process Engineering, Chinese Academy of Sciences, Beijing 100190, China

2 School of Chemical Engineering, University of Chinese Academy of Sciences, Beijing 100049, China

E-mail: zmzhang@ipe.ac.cn

while ionic liquid or glucose as the carbon source [15–16]. Nevertheless, because of the low catalytic activity for the graphitization of molten chlorides, the as-prepared products are amorphous without the detection of local orders, usually referred to as porous carbon instead of graphene [17]. Given the analysis presented, it would be reasonable to anticipate integrating the magnesiothermic reduction approach with the molten salt technique for the sake of capitalizing on their synergistic benefits in the preparation of graphene materials. In fact, the molten salt-assisted magnesiothermic reduction (MSAMR) method has already been widely applied for the preparation of nano-silicon or phosphor-based materials [18], non-ceramic materials [19], and high-purity titanium [20] from their corresponding oxides. Despite all that, to the best of our knowledge, MSAMR has not yet been applied to the synthesis of graphene materials.

In this study, we introduced a facile and up-scalable MSAMR method to synthesize few-layer graphene using alkali carbonate (K_2CO_3) as both the carbon source and the graphitization catalyst besides eutectic alkali chlorides (NaCl–KCl binary system) as the liquid-phase medium. Hereafter the above K_2CO_3-derived few-layer graphene was referred to as *K*-FLG. For comparison, $CaCO_3$-derived few-layer graphene materials with and without molten salts prepared under the same experimental conditions were referred to as *Ca*-FLG and MCG, respectively. To prepare *K*-FLG, both K_2CO_3 and Mg powders were mixed at a stoichiometric ratio and heated in the eutectic molten salt NaCl–KCl at 800 °C for 2 h. *K*-FLG was thus obtained after the elimination of salts and by-products (i.e., MgO and CaO) with deionized water (DIW) and dilute hydrochloric acid, respectively. The detailed experimental process is provided in the ESM of Appendix, and the magnesiothermic reduction is expressed as follows:

$$2Mg + K_2CO_3 \xrightarrow{NaCl-KCl} 2MgO + C + K_2O \quad (1)$$

The morphology and microstructure of *K*-FLG were observed through field-emission scanning electron microscopy (FESEM). It is observed that *K*-FLG has a honeycomb-like morphology (Fig. 1(a)). A closer observation reveals its secondary structure, which is composed of two-dimensional nanosheets with the lateral size and the thickness of 40–150 nm and several nanometers, respectively, as shown in Fig. S1 (included by ESM of Appendix). The detailed structural information was further acquired through transmission electron microscopy (TEM). Figures 1(b) and 1(c) exhibit that the typical structure of *K*-FLG is composed of highly corrugated and interconnected few-layer graphene, forming intertwined scaffolds to provide porous space and hindering the restacking of graphene layers. As revealed by the high-resolution transmission electron microscopy (HRTEM) image in Fig. 1(d), the typical graphene nanosheet of *K*-FLG is composed of 4–8 stacking layers with an interlayer spacing of 0.375 nm, larger than that of the typical Bernal stacking in graphite (0.337 nm), indicating its expanded and turbostratic structure [21]. Interestingly, as a comparison, no obvious lattice fringes are observed for *Ca*-FLG, as shown in Fig. S2 (included by ESM of Appendix), implying that K_2CO_3 can serve as both the carbon source and the catalyst in the graphitization process. Generally, the graphitization of carbon using K_2CO_3 or K_2CO_3-containing molten salts occurs at the temperature of 900 °C, as revealed in Table S1 (included by ESM of Appendix), higher than both the thermal decomposition temperature of K_2CO_3 (i.e., ⩾ 880 °C [22]) and the volatilization temperature of mostly used molten salts (i.e., ⩾ 850 °C [23]). However, due to the high activity of *in-situ* generated carbon in molten salts, the catalytic effect of K_2CO_3 can be achieved at a comparatively lower temperature of 800 °C in this work, which can effectively reduce the loss of molten salts and K_2CO_3.

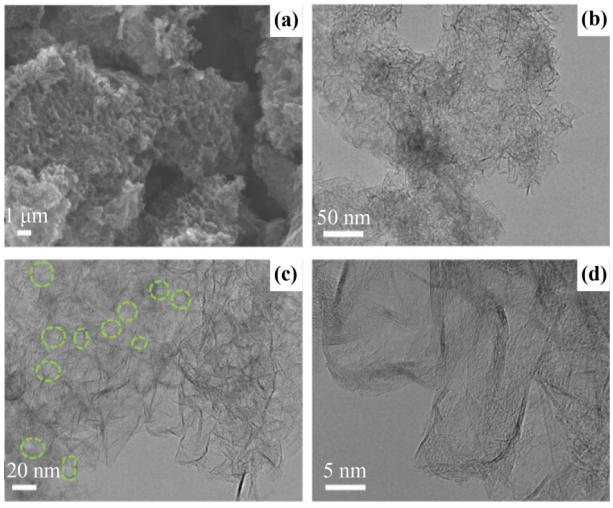

Fig. 1 The morphology and microstructure of *K*-FLG: (**a**) SEM image; (**b**)(**c**) TEM images (revealing several observed mesopores marked with green dot lines); (**d**) HRTEM image.

The porous structure of *K*-FLG was further examined through N_2 adsorption–desorption isotherm measurements, which provided insights into its characteristics like specific surface area (SSA), pore volume, and pore size distribution (PSD). The SSA of *K*-FTG is up to 750 $m^2 \cdot g^{-1}$ according to the Brunauer–Emmett–Teller (BET) method, more than twice that of the thermally reduced graphene oxide (about 350 $m^2 \cdot g^{-1}$ [24]). Figure 2(a) illustrates N_2 adsorption–desorption isotherms for *K*-FLG, displaying type-IV characteristics of mesoporous materials. Moreover, the significant H3 hysteresis loop (according to IUPAC classification) at $0.45p/p_0$–$0.85p/p_0$ and high capillary condensation step indicate uniform and dominant meso-porosity, which agree well with the above TEM observation (Fig. 1(d)). The upright tail at $0.85p/p_0$–$0.99p/p_0$ is attributed to the unsaturated adsorption of the interlayer spacing between graphene sheets. The non-local density functional theory (NLDFT) PSD curve for *K*-FLG in Fig. 2(b) reveals that the mesopores centered at 5.30 and 2.36 nm dominate the pore structure with the additional contribution from micropores centered at 1.43 nm. The most probable pore size of 5.3 nm for *K*-FLG, *Ca*-FLG, and MCG is observed from all PSD curves (the embedded diagram in Fig. 2(b)), indicating that this pore size is independent of the molten salt and the type of carbonates. Thus, the generation of mesopores with the size of 5.3 nm is most likely related to the template effect of MgO generated *in situ*, and pores with sizes of 1.43 and 2.36 nm are associated with molten salts used. Furthermore, Li et al. [10] found that the most probable pore size of graphene obtained through the introduction of CO_2 to liquid Mg at 680 °C was 5.1 nm, extremely similar to our result. The above conclusion further confirms the template effect of MgO generated *in situ*. Thus, the mesopore-dominated structure is well preserved in products after the removal of MgO particles. Meanwhile, the mesopore volume of *K*-FLG is measured to be 1.08 $cm^3 \cdot g^{-1}$, which is large enough to facilitate ion/molecule transportation when applied to energy storage and water purification [25].

To determine the molecular structure of *K*-FLG, Raman spectroscopy was employed. As shown in Fig. 2(c), the spectrum displays three sharp and well-resolved bands peaked approximately at 1340, 1580, and 2675 cm^{-1},

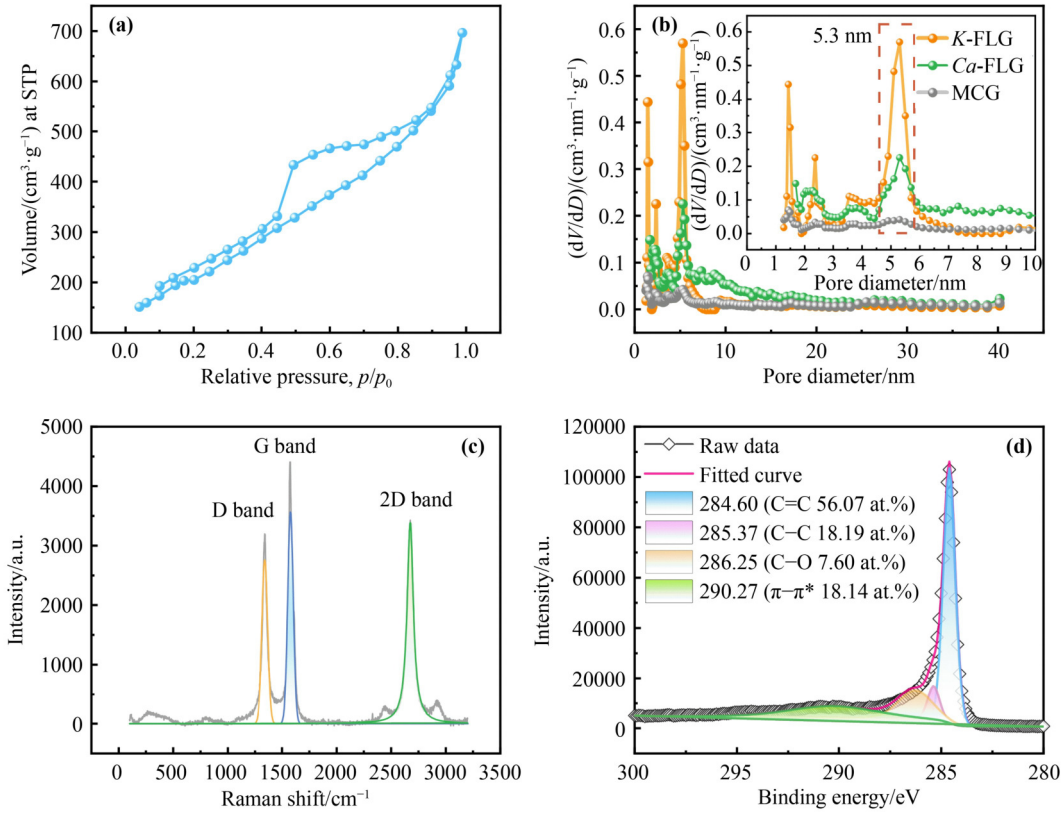

Fig. 2 (**a**) Nitrogen adsorption–desorption isotherms for *K*-FLG. (**b**) Comparison of PSD curves for MCG (grey line), *Ca*-FLG (green line), and *K*-FLG (orange line). (**c**) Raman spectrum for *K*-FLG. (**d**) XPS full spectrum for *K*-FLG together with peak-fitted spectra for C=C, C−C, C−O, and π−π*.

which correspond to D, G, and 2D bands of carbon materials, respectively. The 2D band shifts more towards 2700 cm^{-1} when graphene possesses more than 7–10 layers, which is indistinguishable from graphite [26]. Therefore, *K*-FLG has the few-layer structure, consistent with the above HRTEM observation (Fig. 1(d)). Surprisingly, however, the 2D band accurately fits a single Lorentzian line shape (R^2 = 0.998) or a single Voigt line shape (R^2 = 0.999), as shown in Fig. S3 (included by ESM of Appendix), which is perfectly compliant with characteristics of the single-layer or turbostratic (or misaligned) stacking [27]. Based on above results, it can be inferred that *K*-FLG has the turbostratic (or misaligned) structure with few layers. The comparison of Raman results between *K*-FLG and products obtained via the magnesiothermic reduction (without using molten salts) from various carbon sources is shown in Table S2 (included by ESM of Appendix). It is known that I_D/I_G and I_{2D}/I_G intensity ratios are usually applied to evaluate the disorder degree and the number of layers of graphene materials, respectively. From Table S2, it is observed that the I_D/I_G ratio of *K*-FLG (0.82) is larger than those of products prepared via the self-propagating high-temperature synthesis (SHS) route (0.33–0.81), but smaller than those of products obtained employing other methods (> 1). This can be explained by the fact that the extremely high temperature of reactants during the self-propagating process (close to 2000 °C) leads to the enhancement of graphitization and the decrease of defect concentration. The I_{2D}/I_G ratio of *K*-FLG (1.95) is apparently larger than those of most graphene materials obtained via the magnesiothermic reduction [10−11], proving that *K*-FLG has a smaller number of layers.

Two typical peaks corresponding to different binding energies of C 1s and O 1s are observed in the wide XPS survey scan for *K*-FLG, as shown in Fig. S4(a) (included by ESM of Appendix), with a prominent C 1s peak at 284.6 eV and a small O 1s peak at 532.7 eV. The atomic ratio of carbon to oxygen (C/O) for *K*-FLG is 32, much larger than that of graphene prepared through the reduction of graphene oxide (i.e., < 15) [13] as well as those from most reported studies summarized in Table S3 (included by ESM of Appendix). The larger C/O ratio is attributed to the strong deoxidation of magnesium in molten salt (i.e., the partial dissolution and the ionization of magnesium improve its reducing capacity [28]), beneficial for the transportation of electrons in graphene materials. Moreover, the C 1s spectrum was deconvoluted into four peaks (Fig. 2(d)) with binding energies of 284.60, 285.37, 286.25, and 290.27 eV, which correspond to C=C (sp^2) (56.07 at.%), C−C (sp^3) (18.19 at.%), C−O (7.60 at.%), and π−π* (18.14 at.%), respectively. It is noteworthy that the sp^2 conjugated carbon predominates with a minor contribution from oxygenated carbons. Compared with that for *Ca*-FLG (with contents of the sp^2 hybridized carbon at 49.24 at.% and the sp^3 hybridized carbon at 32.47 at.%), the content of the sp^3 hybridized carbon for *K*-FLG sharply decreases, implying the improvement of graphitization due to the use of K_2CO_3, consistent with X-ray diffraction (XRD) results in Fig. S4(b) (included by ESM of Appendix).

Based on above analysis, the formation process of *K*-FLG can be deduced as follows (Fig. 3): At first, K_2CO_3 dissolves in the NaCl–KCl eutectic molten salt at above 650 °C forming a homogeneous ionic liquid [29]. After that, the chemical reaction between Mg and K_2CO_3 occurs according to Eq. (1), which can be confirmed through the thermodynamic calculation ($\Delta_r G$ = −339 kJ·mol^{-1}, $\Delta_r H$ = −411 kJ·mol^{-1}, 800 °C) and the product observation in Fig. S5 (included by ESM of Appendix). Subsequently, carbon atoms generated spontaneously organize themselves on the surface of *in-situ* formed MgO nanoparticles, where a large amount of sp^2 hybrid carbons are structured into many graphite microcrystals interconnected by sp^3 cross-linking bonds [30]. Due to the relatively higher chemical activity compared with that of sp^2 hybridized carbons, sp^3 hybridized carbons are preferentially consumed by K_2CO_3 at above 700 °C (Eq. (2)) [31]. Finally, sp^2 microcrystals are released from the constraint of cross-linked sp^3 carbons, move freely in molten salts, and are interconnected with each other to form a large graphene layer, following the principle of lowest energy. Potassium atoms are generated according to Eqs. (2) and (3) expressed as follows:

$$2C + K_2CO_3 \rightarrow 2K + 3CO \quad (2)$$

$$C + K_2O \rightarrow 2K + CO \quad (3)$$

which further form charge-transfer complexes with sp^2 microcrystals, akin to polycyclic aromatic hydrocarbons, thereby enhancing the catalytic graphitization and accelerating the formation of graphene layers [32].

In summary, few-layer graphene, characterized with a 4–8 stacking layered, mesopor-dominated, and turbostractic microstructure as well as a high degree of

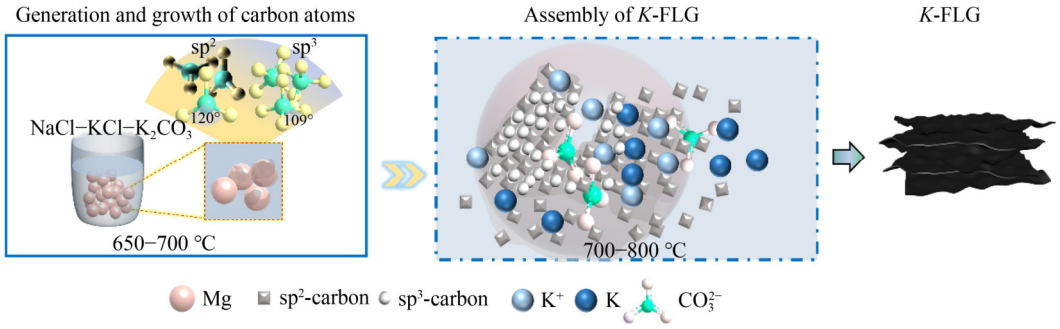

Fig. 3 Schematic representation of the formation mechanism of *K*-FLG.

graphitization, was prepared via MSAMR from K_2CO_3. The synergistic effects of K_2CO_3 (as both the carbon source and the graphitization catalyst), *in-situ* generated MgO (as the template), and NaCl–KCl (as the eutectic molten salt preventing the Bernal stacking of graphene layers) enable the fabrication of few-layer graphene at a relatively low temperature.

Declaration of competing interests The authors declare no conflict of interests.

Acknowledgements We would like to acknowledge the funding support from the National Natural Science Foundation of China (Grant No. 22278404).

Online appendix Electronic supplementary material (ESM) can be found in the online version at https://doi.org/10.1007/s11706-025-0722-3 and https://journal.hep.com.cn/foms/EN/10.1007/s11706-025-0722-3 that includes Figs. S1–S5 and Table S1–S3.

Received February 5, 2025; accepted March 6, 2025

References

[1] Luong D X, Bets K V, Algozeeb W A, et al. Gram-scale bottom-up flash graphene synthesis. Nature, 2020, 577(7792): 647−651

[2] Oh M, Nuckolls K P, Wong D, et al. Evidence for unconventional superconductivity in twisted bilayer graphene. Nature, 2021, 600(7888): 240−245

[3] Yang J, Li M, Fang S, et al. Water-induced strong isotropic MXene-bridged graphene sheets for electrochemical energy storage. Science, 2024, 383(6684): 771−777

[4] Carrasco D F, Álvarez-Rubiera E, Villar-Rodil S, et al. Chemically tuning graphene via anodic exfoliation for enhanced performance in aqueous zinc-based electrochemical energy storage applications. Carbon, 2024, 228: 119293

[5] Shen C, Qing F, Li X. The etching effect of oxygen during the cooling process of graphene CVD synthesis. Carbon, 2024, 230: 119654

[6] Xing Z, Wang B, Halsted J K, et al. Direct fabrication of nanoporous graphene from graphene oxide by adding a gasification agent to a magnesiothermic reaction. Chemical Communications, 2015, 51(10): 1969−1971

[7] Wang J, Xu X, Cheng T, et al. Dual-coupling-guided epitaxial growth of wafer-scale single-crystal WS_2 monolayer on vicinal *a*-plane sapphire. Nature Nanotechnology, 2022, 17(1): 33−38

[8] Moreno C, Vilas-Varela M, Kretz B, et al. Bottom-up synthesis of multifunctional nanoporous graphene. Science, 2018, 360(6385): 199−203

[9] Zhang Q, Yan B, Feng L, et al. Progress in the use of organic potassium salts for the synthesis of porous carbon nanomaterials: microstructure engineering for advanced supercapacitors. Nanoscale, 2022, 14(23): 8216−8244

[10] Li X J, Wang X J, Hu X S, et al. Direct conversion of CO_2 to graphene via vapor–liquid reaction for magnesium matrix composites with structural and functional properties. Journal of Magnesium and Alloys, 2023, 11(4): 1206−1212

[11] Yin H, Chen P, Xu C, et al. Shock-wave synthesis of multilayer graphene and nitrogen-doped graphene materials from carbonate. Carbon, 2015, 94: 928−935

[12] Zhao J, Guo Y, Li Z, et al. An approach for synthesizing graphene with calcium carbonate and magnesium. Carbon, 2012, 50(13): 4939−4944

[13] Tang H, Gao P, Liu X, et al. Bio-derived calcite as a sustainable source for graphene as high-performance electrode material for energy storage. Journal of Materials Chemistry A: Materials for Energy and Sustainability, 2014, 2(38): 15734−15739

[14] Dyjak S, Kiciński W, Norek M, et al. Hierarchical, nanoporous graphenic carbon materials through an instant, self-sustaining magnesiothermic reduction. Carbon, 2016, 96: 937−946

[15] Fechler N, Fellinger T P, Antonietti M. “Salt templating”: a simple and sustainable pathway toward highly porous functional carbons from ionic liquids. Advanced Materials, 2013, 25(1): 75−79

[16] Fechler N, Zussblatt N P, Rothe R, et al. Eutectic syntheses of graphitic carbon with high pyrazinic nitrogen content. Advanced Materials, 2016, 28(6): 1287−1294

[17] Du X, Lin Z, Zhang Y, et al. Microstructural tailoring of porous few-layer graphene-like biochar from kitchen waste hydrolysis residue in molten carbonate medium: structural evolution and conductive additive-free supercapacitor application. Science of the Total Environment, 2023, 871: 162045

[18] Zhu L, Zhu Z, Zhou J, et al. Kirkendall effect modulated hollow red phosphorus nanospheres for high performance sodium-ion battery anodes. Chemical Communications, 2020, 56(79): 11795−11798

[19] Ye B, Fan C, Han Y, et al. Synthesis of high-entropy diboride nanopowders via molten salt-mediated magnesiothermic reduction. Journal of the American Ceramic Society, 2020, 103(9): 4738−4741

[20] Fang Z Z, Middlemas S, Guo J, et al. A new, energy-efficient chemical pathway for extracting Ti metal from Ti minerals. Journal of the American Chemical Society, 2013, 135(49): 18248−18251

[21] Athanasiou M, Samartzis N, Sygellou L, et al. High-quality laser-assisted biomass-based turbostratic graphene for high-performance supercapacitors. Carbon, 2021, 172: 750−761

[22] Wu Y, Ren N, Wang T, et al. Experimental study on optimized composition of mixed carbonate salt for sensible heat storage in solar thermal power plant. Solar Energy, 2011, 85(9): 1957−1966

[23] Pang Z Y, Li G S, Xiong X L, et al. Molten salt synthesis of porous carbon and its application in supercapacitors: a review. Journal of Energy Chemistry, 2021, 61: 622−640

[24] Yan J, Wang Q, Wei T, et al. Template-assisted low temperature synthesis of functionalized graphene for ultrahigh volumetric performance supercapacitors. ACS Nano, 2014, 8(5): 4720−4729

[25] Jayaramulu K, Dubal D P, Nagar B, et al. Ultrathin hierarchical porous carbon nanosheets for high-performance supercapacitors and redox electrolyte energy storage. Advanced Materials, 2018, 30(15): 1705789

[26] Ferrari A C, Meyer J C, Scardaci V, et al. Raman spectrum of graphene and graphene layers. Physical Review Letters, 2006, 97(18): 187401

[27] Roscher S, Hoffmann R, Ambacher O. Determination of the graphene–graphite ratio of graphene powder by Raman 2D band symmetry analysis. Analytical Methods, 2019, 11(9): 1224−1228

[28] Zhang Y, Fang Z Z, Sun P, et al. Kinetically enhanced metallothermic redox of TiO_2 by Mg in molten salt. Chemical Engineering Journal, 2017, 327: 169−182

[29] Yaokawa J, Oikawa K, Anzai K. Thermodynamic assessment of the KCl–K_2CO_3–NaCl–Na_2CO_3 system. Calphad, 2007, 31(2): 155−163

[30] Nanaji K, Sarada B V, Varadaraju U V, et al. A novel approach to synthesize porous graphene sheets by exploring KOH as pore inducing agent as well as a catalyst for supercapacitors with ultra-fast rate capability. Renewable Energy, 2021, 172: 502−513

[31] Hao P, Zhao Z H, Leng Y H, et al. Graphene-based nitrogen self-doped hierarchical porous carbon aerogels derived from chitosan for high performance supercapacitors. Nano Energy, 2015, 15: 9−23

[32] Xia M, Chen W, Wu J, et al. The critical role of anions in the porous biochar structure and potassium release during the potassium-assisted pyrolysis process. Green Chemistry, 2021, 23(23): 9589−9599